*Bulletin of Computational Intelligence*
https://www.sciltp.com/journals/bci

*Article*

# An Integrated Multi-Criteria Risk-Assessment Framework for Rockburst in Underground Construction

Shahab Hosseini [1], Nakhshin Jasimi [1], Bahar Mehdizadeh [2], Manoj Khandelwal [3], Ramesh Murlidhar Bhatawdekar [4], Pejman Sabet [5], Masoud Monjezi [1], Seyed Yaser Mousavi Siamakani [6] and Danial Jahed Armaghani [7,*]

[1] Department of Mining Engineering, Faculty of Engineering, Tarbiat Modares University, Tehran 1411944961, Iran
[2] School of Engineering, Macquarie University, Sydney, NSW 2113, Australia
[3] Institute of Innovation, Science and Sustainability, Federation University Australia, Ballarat, VIC 3350, Australia
[4] Geotropik, Faculty of Civil Engineering, Universiti Teknologi Malaysia, Skudai, Johor Bahru 81310, Malaysia
[5] Engineering Design and Construction, Acknowledge Education, Melbourne, VIC 3000, Australia
[6] College of Engineering, Department of Civil Engineering, Rangsit University, Mueang, Pathum Thani 12000, Thailand
[7] School of Civil and Environmental Engineering, University of Technology Sydney, Sydney, NSW 2007, Australia
* Correspondence: danial.jahedarmaghani@uts.edu.au

**How To Cite:** Hosseini, S.; Jasimi, N.; Mehdizadeh, B.; et al. An Integrated Multi-Criteria Risk-Assessment Framework for Rockburst in Underground Construction. *Bulletin of Computational Intelligence* **2026**, *2*(2), 181–195. https://doi.org/10.53941/bci.2026.100010

Received: 18 December 2025
Revised: 6 May 2026
Accepted: 7 May 2026
Published: 20 May 2026

**Abstract:** Rockburst is among the most critical hazards in underground construction, and it is caused by complex interactions among in-situ stress, rock mass conditions and excavation processes. This study proposes an integrated multi-criteria risk-assessment framework that combines failure mode and effects analysis (FMEA); value-function modelling; and the combined compromise solution (CoCoSo) methods to analyse ruckburst risk. Unlike existing rockburst risk-assessment approaches that rely on single aggregation schemes or purely predictive models, the proposed framework enables robust and consistent prioritisation of failure modes by incorporating expert judgement, multiple value-function mappings and compromise-based decision aggregation. Six weighted criteria—severity, occurrence likelihood, detection difficulty, cost, response timeliness and success likelihood—were applied to 20 representative rockburst-related failure modes. The results consistently identify microcrack development, ground-anchor failure, stress redistribution and support failure as the most critical risks across all aggregation schemes. The proposed framework provides a practical decision-support tool for underground construction projects, supporting targeted monitoring, optimised support design and proactive risk-mitigation strategies.

**Keywords:** rockburst; tunnelling and underground construction; risk analysis; multi-criteria decision-making; failure mode and effects analysis

## 1. Introduction

Underground construction projects, including tunnelling and mining operations, routinely grapple with the unpredictable and potentially catastrophic phenomenon of rockburst. Rockburst manifests as sudden, violent failures of rock under high in-situ stress, often accompanied by the ejection of rock fragments, spalling of the tunnel lining, and intense seismic energy release [1]. Such events pose severe threats to worker safety, equipment integrity and schedule continuity, and can incur substantial remediation costs and operational delays [2,3]. Despite advances in real-time monitoring and support technologies, accurately predicting when and where a rockburst will occur remains a formidable challenge because of the complex interplay among the factors of geological heterogeneity, stress redistribution around excavations, and excavation sequencing [4].

Artificial intelligence techniques constitute a significant component of contemporary methods for addressing complex problems in rock mechanics and underground construction [5–10]. For example, to predict rockburst, several researchers have proposed artificial intelligence techniques such as fuzzy system [11,12]; support vector machine [3]; Catboost [13]; and hybrid artificial neural network [14]. Such studies proposed models that can determine whether there is rockburst by analysing the real data. While these approaches demonstrate promising predictive capability, they do not provide structured prioritisation of risk dimensions before rockburst occurrence. This limitation highlights the need for a structured multi-criteria risk-assessment framework capable of systematically integrating multiple risk dimensions to identify the risk of rockburst before it occurs. It is important to mention that many problems involved in civil and mining engineering have been solved by artificial intelligent techniques [15–19].

Traditional risk-assessment approaches for rockburst bifurcate into qualitative expert-judgement frameworks, such as hazard checklists and categorical risk matrices, and quantitative indices grounded in seismic magnitude thresholds, energy release calculations, or empirical rock mass classification systems [11]. While qualitative methods offer rapid, experience-based prioritisation, they are often subjective and lack reproducibility. However, purely quantitative models demand extensive calibration data and may not fully capture emergent, site-specific interactions among multiple risk factors. Furthermore, single-criterion or single-metric approaches can obscure the relative importance of safety, cost, detectability and response time in a comprehensive risk profile.

Although previous studies have combined failure mode and effects analysis (FMEA) with single multi-criteria decision-making (MCDM) techniques (e.g., TOPSIS [Technique for Order of Preference by Similarity to Ideal Solution]; or analytic hierarchy process) to improve risk prioritisation, these approaches typically rely on a single aggregation logic and do not examine the robustness of rankings under alternative transformation schemes. The primary contribution of the present study lies not merely in integrating FMEA with an additional decision-making method, but in developing a robustness-oriented multi-aggregation framework. Specifically, we introduce 12 distinct value-function mappings (linear, piecewise, stepwise and exponential) alongside the combined compromise solution (CoCoSo) method and systematically evaluate ranking stability across 14 aggregation schemes. This stability-validated structure ensures that the identification of critical rockburst-related failure modes is not an artefact of a specific aggregation assumption. To the best of the authors' knowledge, such a multimapping robustness assessment has not been previously applied in studies of rockburst risk prioritisation.

Despite the growing body of research on rockburst prediction and hazard modelling, several methodological gaps remain in the existing literature. Existing studies predominantly focus on classifying or forecasting rockburst occurrence using machine learning and artificial intelligence techniques. While these approaches demonstrate promising predictive performance, they do not inherently provide structured prioritisation of multidimensional risk factors prior to rockburst occurrence.

In addition, previous FMEA–MCDM hybrid frameworks proposed in underground construction studies typically rely on a single aggregation mechanism. Such approaches address limitations of traditional risk priority number (RPN) but do not assess whether ranking results remain stable under alternative transformation assumptions. Consequently, the robustness of prioritisation outcomes remains largely unverified in the existing literature.

The present study addresses this conceptual and methodological gap by introducing a robustness-oriented multi-aggregation framework. Rather than replacing classic FMEA with a single decision-making technique, the proposed model integrates 12 value-function mappings and the CoCoSo method within a unified structure and systematically evaluates ranking stability across 14 aggregation schemes. This multi-layer validation ensures that the identification of critical rockburst-related failure modes is not an artefact of a specific transformation or aggregation logic. Therefore, the main contribution of this study lies not only in applying multi-criteria analysis to rockburst risk but in establishing a stability-validated prioritisation architecture that enhances methodological transparency and reliability in underground hazard assessment.

To address these gaps in research, this study proposes a unified, multi-criteria risk-assessment framework that integrates classic FMEA with a family of mathematical value-function mappings and a CoCoSo technique. The following six expert-elicited criteria were used to score 20 representative failure modes spanning the spectrum from microcrack initiation to full roof collapse and system failures: severity, occurrence likelihood, detection difficulty, cost of mitigation, response timeliness, and success likelihood. By applying 12 distinct piecewise and continuous value functions (including simple linear and exponential forms) and comparing results with both FMEA-derived RPNs and CoCoSo indices, we demonstrate a robust convergence in prioritisation. The proposed method not only enhances transparency and repeatability but also allows practitioners to tailor the risk-scoring process to project-specific thresholds, such as hard safety cut-offs or gradual escalation curves, without altering the core ranking of critical hazards. This flexible, expert-guided framework thus provides a powerful decision-

support tool for improving safety, optimising resource allocation and mitigating rockburst risk in complex underground environments.

## 2. Research Method

The proposed methodological structure integrates FMEA, value-function transformations and the CoCoSo compromise aggregation within a unified framework. The integration of these three analytical methods is not intended to increase procedural complexity, but to address the distinct methodological limitations observed in conventional risk-prioritisation models.

FMEA provides a systematic mechanism for identifying failure modes and structuring multidimensional risk criteria. However, classic RPN aggregation assumes direct multiplicative interaction and fixed linear interpretability of scores. Second, value-function mappings are introduced to relax strict linearity assumptions and examine how alternative transformation profiles (linear, piecewise, stepwise and exponential) influence prioritisation outcomes. This step enables sensitivity evaluation at the transformation level. Third, the CoCoSo method is employed as a compromise-based aggregation approach to mitigate potential dominance effects inherent in multiplicative RPN scoring. CoCoSo balances additive and multiplicative normalisation logic, providing an alternative ranking structure for robustness comparison. Together, these components form a stability-oriented multi-aggregation architecture that ensures the final prioritisation is not dependent on a single scoring or transformation assumption.

This study develops and compares four complementary risk-assessment approaches, classic FMEA; piecewise linear value-function modelling (including simple linear and exponential mappings); and the CoCoSo method, applied to 20 key failure modes in underground construction. The adopted methodology is explained in the following subsections.

### *2.1. Identification and Characterisation of Failure Modes*

An initial screening of tunnelling incident reports, geomechanical studies and expert interviews yielded 20 failure modes (FM1–FM20), which capture the progression of rockburst hazards from early warning signs to catastrophic collapse and downstream system effects. FM1 refers to the ultimate safety concern (risk of injury or death to personnel). FM2 refers to sudden rock failure that ejects fragments into the excavation. FM3 refers to the collapse or failure of the tunnel roof. FM4 refers to the release of seismic energy in the form of microseismic events. FM5 refers to structural reinforcement vulnerabilities (e.g., failure of permanent support structures such as rock bolts and mesh). FM10 refers to failure of temporary supports such as shotcrete or steel ribs. FM11 refers to the failure of ground anchors or cable bolts. FM6 refers to progressive damage to the lining (e.g., severe cracking in walls and ceilings. FM12 refers to the spalling of the rock surface. FM8 refers to stress-related precursors (e.g., development of microcracks). FM7 refers to delayed rockburst due to stress redistribution. FM9 refers to slow, time-dependent deformation under sustained loads (i.e., rock creep). FM13 refers to hydromechanical effects (e.g., damage to tunnel water supply or drainage). FM14 refers to groundwater intrusion through stress-induced cracks. FM15 refers to operational and emergency considerations (e.g., blockage of escape routes). FM20 refers to sudden halt in drilling or extraction operations. FM16 (damage to underground communication systems); FM17 (failure of stress and pressure monitoring systems); FM18 (entrapment or damage to drilling machinery); and FM19 (vibration-induced equipment malfunction) refer to the cascading effects on control systems and equipment reliability. This comprehensive set of 20 failure modes ensures that our subsequent multi-criteria analysis fully reflects both the geomechanical triggers of rockburst and their critical safety and operational consequences. These failure modes were taken from an earlier study by the same research group [11,20].

### *2.2. Expert-Driven Criteria Weighting*

Six evaluation criteria, severity (S), occurrence likelihood (O), detection difficulty (D), remediation cost (C), response timeliness (T), and success likelihood (Su), were selected based on industry best practices and prior literature. A panel of eight senior geomechanics and tunnelling experts participated in a Delphi-style elicitation to assign relative importance to each criterion. Through iterative feedback and convergence, normalised weights were obtained.

The expert panel consisted of eight senior professionals selected based on predefined eligibility criteria, including minimum professional experience, domain expertise and prior involvement in underground or rockburst-related projects. The anonymised profile of the panel members is summarised in Table 1.

As presented in Table 1, the panel reflects balanced representation from both academia and industry, with all experts possessing more than 12 years of relevant experience and direct exposure to rockburst-prone underground environments. This diversity enhances the credibility and practical relevance of the elicited judgements.

**Table 1.** Profile of expert panel involved in Delphi weighting process.

| Expert ID | Sector | Primary Expertise | Years of Experience | Role |
|---|---|---|---|---|
| E1 | Academia | Rock Mechanics | 18 | Professor |
| E2 | Industry | Underground Mining | 22 | Technical Director |
| E3 | Academia | Geotechnical Engineering | 15 | Associate Professor |
| E4 | Industry | Tunnel Construction | 20 | Senior Engineer |
| E5 | Academia | Seismic Rock Behaviour | 14 | Research Scientist |
| E6 | Industry | Ground Support Design | 17 | Project Manager |
| E7 | Academia | Risk Assessment | 12 | Lecturer |
| E8 | Industry | Deep Mining Operations | 25 | Mine Planning Specialist |

### *2.3. FMEA-Based RPN Calculation*

In the first approach, each failure mode (FM1–FM20) was scored on the six criteria using a 1–10 scale [7]. The composite RPN was then computed as the product, and the modes were ranked in descending RPN order. This method provides an intuitive baseline for identifying high-risk scenarios [8]:

$$RPN = S \times O \times D \times C \times T \times Su'$$

The six-factor multiplicative RPN adopted in this study extends the classic FMEA structure; however, it is important to acknowledge the limitations of RPN formulations here. That is, multiplicative aggregation may generate identical RPN values for distinct risk profiles (non-uniqueness); assumes proportional interaction among criteria; and treats ordinal scores as implicitly interval-scaled quantities. Moreover, increasing the number of multiplicative dimensions may amplify sensitivity to extreme values, potentially exaggerating dominance effects. For this reason, the six-factor RPN is employed as a structured baseline reference rather than a definitive prioritisation mechanism. The subsequent application of value-function mappings and CoCoSo compromise aggregation is specifically intended to mitigate these limitations and evaluate ranking robustness beyond the classic multiplicative assumption [21,22].

Although success likelihood (Su) represents mitigation effectiveness and is conceptually a benefit-type criterion, it was transformed before performing multiplicative aggregation in the extended RPN formulation to preserve directional consistency. Specifically, an inverse transformation was applied such that higher mitigation success corresponds to lower risk contribution. For the FMEA-based calculation, the adjusted term was defined as Su' = 11, with Su ensuring that higher mitigation effectiveness reduces the composite risk score. Similarly, in value-function and CoCoSo aggregations, Su was treated as a benefit-type criterion and normalised using decreasing transformation functions [23].

To ensure transparency and reproducibility of the expert scoring process, explicit rating anchors were defined for the 1–10 scale applied to all six criteria as shown in Table 2. These anchors provide qualitative descriptors and practical examples for low, medium and extreme levels of each criterion, thereby minimising ambiguity in interpretation among experts.

During the Delphi-style elicitation process, experts independently assigned scores in the first round. The median value for each criterion was provisionally adopted. Consensus was considered achieved when the interquartile range (IQR) was ≤1. In cases where dispersion exceeded this threshold, structured feedback and clarification were provided, followed by a second scoring round. The final failure mode scores correspond to the median values obtained after convergence.

In the proposed framework, explicit directionality was assigned to all six criteria to ensure aggregation consistency. Severity (S), occurrence likelihood (O), detection difficulty (D), remediation cost (C), and response timeliness (T) were treated as cost-type (risk-increasing) criteria, meaning higher scores correspond to greater risk.

In contrast, success likelihood (Su), representing the probability of effective mitigation, was treated as a benefit-type (risk-reducing) criterion, where higher values indicate improved mitigation capability and therefore reduce overall risk.

Accordingly, during normalisation and value-function transformations, cost-type criteria were mapped using increasing risk functions, whereas the benefit-type criterion (Su) was transformed using a decreasing function to maintain directional consistency. This ensures that, in all aggregation methods (FMEA, value-function models and CoCoSo), higher composite scores consistently correspond to higher overall risk levels.

**Table 2.** Rating guidelines for the 1–10 evaluation scale.

| Mark | Rate | Linguistic Variables | Linguistic Variables | Severity (S) | Occurrence Likelihood (O) | Detection Difficulty (D) | Cost (C) | Time (T) | Success Likelihood (Su) |
|---|---|---|---|---|---|---|---|---|---|
| R1 | 1 | Extremely high (EH) | Extremely high (EH) | Failure is hazardous and causes system failure | Extremely high: Failure almost inevitable | Design control cannot detect failures | Without cost | Without time | Full success |
| R2 | 2 | Very high (VH) | Very high (VH) | Failure involves hazardous outcomes | Very high | Very remote chance of detecting failures | Very low | Very low | Extreme success |
| R3 | 3 | Relatively high (RH) | Relatively high (RH) | System is inoperable with loss of primary function | High | Remote chance of detecting failures | Low | Low | Very high success |
| R4 | 4 | High (H) | High (H) | System performance is severely affected but functions | Moderately high | Very low chance to detect failures | Relatively low | Relatively low | High success |
| R5 | 5 | Moderately high (MH) | Moderately high (MH) | System performance is degraded; comfort functions may not operate | Moderate | Low chance of detecting failures | Moderate | Moderate | Medium–high success |
| R6 | 6 | Moderate (M) | Moderate (M) | Moderate effect on system performance; requires repair | Moderate | Moderate chance of detecting failures | Moderately high | Moderately high | Medium success |
| R7 | 7 | Relatively low (RL) | Relatively low (RL) | Small effect on system performance; no repair needed | Relatively low | Good chance of detecting failures | High | High | Medium–low success |
| R8 | 8 | Low (L) | Low (L) | Minor effect on system performance | Low | High chance of detecting failures | Relatively high | Relatively high | Low success |
| R9 | 9 | Very low (VL) | Very low (VL) | Very minor effect on system performance | Remote | Very high chance of detecting failures | Very high | Very high | Very low success |
| R10 | 10 | None (N) | None (N) | No effect; nearly impossible | Nearly impossible | Design control will almost certainly detect failures | Extremely high | Extremely high | Without success |

### *2.4. Value-Function Mapping*

To introduce non-linearity and threshold effects, we defined 12 value functions that map raw criterion scores (1–10) to normalised [0, 1] values:

- piecewise linear: increasing, decreasing, V-shape, inverted V-shape, increase-level, level-decrease, level-increase, decrease-level
- stepwise: increasing and decreasing
- continuous: simple linear and exponential ($\alpha = 0.3$)

Each failure mode's criterion value was transformed via one mapping at a time, then aggregated using the expert weights:

$$Score = \sum_{k \in S,O,D,C,T,Su} \left( \omega_k \times v_k \right)$$

where $v_k$ is the mapped value and $w_k$ the corresponding weight. This process yielded 14 ranking lists, one for each mapping plus the simple-linear, exponential, FMEA and CoCoSo outcomes, enabling sensitivity analysis of the ranking process to different functional forms.

To provide a visual interpretation of the functional transformations applied to the raw 1–10 criterion scores, Figure 1 illustrates the graphical behaviour of the principal value-function mappings used in this study.

All six criteria were scored using a uniform 1–10 ordinal scale with consistent resolution across dimensions. While equal numerical spacing was maintained for practical comparability, the raw scores were not assumed to represent strictly linear interval properties. To address potential non-linearity in risk perception and criterion interpretation, multiple value-function mappings (linear, piecewise, stepwise and exponential) were applied during aggregation. This approach allows the framework to relax strict linear interpretability assumptions at the scoring stage while preserving consistency in resolution across criteria.

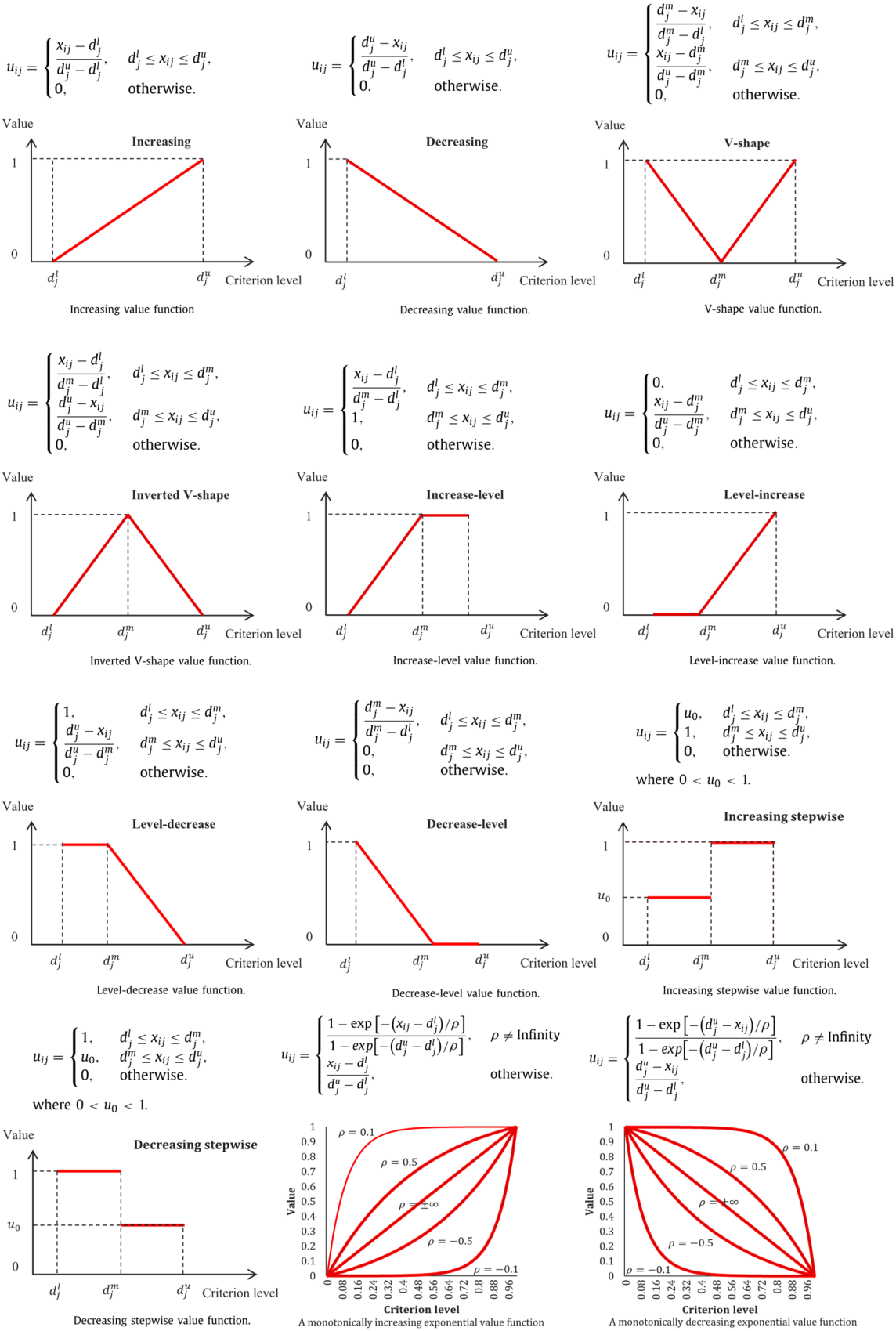


**Figure 1.** Graphical representation of the value-function mappings.

## *2.5. CoCoSo*

As a final MCDM alternative, the CoCoSo technique [9] generates three intermediate aggregates for each alternative *i*:

1. additive sum $\xi_a$: the weighted sum of criterion values

2. multiplicative product $\xi_b$ : the weighted geometric product
3. compromise aggregate $\xi_c$: a balanced compromise between additive and multiplicative effects.

The overall CoCoSo index was used to rank failure modes. This hybrid approach reconciles the complementary advantages of sum-based and product-based aggregations.

$$\xi_i = \frac{1}{3}\left(\xi_i^a + \xi_i^b + \xi_i^c\right)$$

By juxtaposing classic FMEA, piecewise value-function models and CoCoSo, our method offers a robust, transparent and flexible framework for multi-criteria risk prioritisation in underground construction that can accommodate both expert judgement and data-driven transformations.

Several methodological design choices in the present framework require clarification, particularly the selection of the six evaluation criteria; the inclusion of success likelihood (Su); and the adoption of 12 value-function mappings.

First, the six criteria (severity, occurrence likelihood, detection difficulty, cost, response timeliness, and success likelihood) were selected to extend classic FMEA dimensions into a broader operational and economic risk context. While traditional FMEA relies on severity, occurrence and detection, underground rockburst risk involves additional project-specific consequences such as economic losses (cost) and intervention timing (response timeliness). These dimensions are frequently highlighted in underground construction and mining-risk literature. The inclusion of success likelihood (Su) reflects mitigation effectiveness and recovery capacity. Unlike traditional damage-oriented parameters, Su captures the probability that implemented control measures can successfully reduce risk and the negative outcomes of failures. This addition allows the framework to incorporate resilience considerations, aligning risk prioritisation with proactive risk-management principles.

Second, the 12 value-function mappings were selected to systematically represent common transformation families used in MCDM, including linear, piecewise, stepwise, V-shaped, inverted V-shaped and exponential forms. These mappings were not arbitrarily chosen but were intended to span monotonic increasing, monotonic decreasing and non-monotonic response behaviours. By covering this structured transformation space, the study evaluates whether ranking outcomes remain stable under diverse functional assumptions.

The purpose of including multiple mappings is therefore not methodological inflation, but robustness validation. The convergence of ranking results across these transformation families strengthens confidence that the prioritisation structure does not depend on a single modelling assumption.

## 3. Results of the Models

### *3.1. FMEA*

In the extended FMEA assessment (Table 3), the computed RPNs integrate six evaluation criteria (S, O, D, C, T and Su) to yield a comprehensive ranking of failure modes by criticality. At the apex of this ranking, FM8 (Table 3) attains an RPN of 315,000, closely followed by FM10 at 313,600. Both modes combine very high severity ratings (S = 7–10) with challenging detectability (D = 10 for FM8; D = 8 for FM10); substantial corrective costs (C = 10 for FM8; C = 8 for FM10); and critical time windows for intervention (T = 10 and 7, respectively). Their elevated ‘success’ scores (Su = 9 and 7) indicate that, although effective countermeasures exist, timely deployment is paramount, a finding that underscores the need for advanced microseismic monitoring and rapid-response support systems in zones prone to sudden stress release.

FM7 emerges as the third-highest risk (RPN = 240,000), driven by its peak detectability challenge (D = 10); maximal intervention cost and time demands (C = T = 10); and strong mitigation potential (Su = 8). This profile points to an urgent requirement for real-time geomechanical instrumentation and adaptive support designs capable of responding to evolving in-situ stress fields.

Intermediate RPN values differentiate a second tier of concerns—FM5 (‘Failure of permanent support structures’; RPN = 69,120) and FM4 (‘Release of seismic energy’; RPN = 56,700). Although their S and O ratings are similarly high, their comparatively lower detection and response burdens allow for targeted design optimisations and periodic reinforcement cycles rather than continuous intervention.

In contrast, failure modes such as FM3 (‘Collapse or failure of tunnel roof’; RPN = 4800) and FM6 (‘Severe cracking in tunnel walls and ceilings’; RPN = 5376) register RPNs less than 10,000, reflecting manageable severity levels or detection ease that justify routine inspection regimes and standard maintenance protocols.

**Table 3.** Results of FMEA method and calculated RPN score.

| Failure Mode | S | O | D | C | T | Su | RPN | Rank |
|---|---|---|---|---|---|---|---|---|
| FM1 | 3 | 5 | 9 | 5 | 5 | 2 | 6750 | 11 |
| FM2 | 4 | 4 | 6 | 6 | 5 | 2 | 5760 | 12 |
| FM3 | 4 | 5 | 10 | 2 | 4 | 3 | 4800 | 14 |
| FM4 | 7 | 9 | 10 | 6 | 5 | 3 | 56,700 | 6 |
| FM5 | 8 | 9 | 10 | 8 | 3 | 4 | 69,120 | 5 |
| FM6 | 4 | 7 | 6 | 8 | 2 | 2 | 5376 | 13 |
| FM7 | 6 | 5 | 10 | 10 | 10 | 8 | 240,000 | 4 |
| FM8 | 7 | 5 | 10 | 10 | 10 | 9 | 315,000 | 2 |
| FM9 | 7 | 5 | 8 | 7 | 5 | 1 | 9800 | 9 |
| FM10 | 10 | 10 | 8 | 8 | 7 | 7 | 313,600 | 3 |
| FM11 | 9 | 10 | 10 | 8 | 9 | 7 | 453,600 | 1 |
| FM12 | 4 | 5 | 7 | 1 | 1 | 3 | 420 | 15 |
| FM13 | 1 | 6 | 7 | 1 | 2 | 1 | 84 | 19 |
| FM14 | 2 | 5 | 5 | 3 | 2 | 1 | 300 | 16 |
| FM15 | 4 | 2 | 6 | 2 | 1 | 3 | 288 | 17 |
| FM16 | 1 | 2 | 6 | 2 | 1 | 1 | 24 | 20 |
| FM17 | 5 | 1 | 6 | 3 | 2 | 1 | 180 | 18 |
| FM18 | 6 | 5 | 8 | 4 | 3 | 3 | 8640 | 10 |
| FM19 | 4 | 5 | 9 | 5 | 3 | 6 | 16,200 | 8 |
| FM20 | 5 | 6 | 8 | 3 | 4 | 8 | 23,040 | 7 |

### *3.2. Piecewise Linear Value Functions*

In the context of piecewise linear value functions, these expert-elicited weights are indispensable. While the piecewise mappings transform each raw criterion score into a value on the [0, 1] interval according to predefined breakpoints and slopes, the weights ensure that when these values are aggregated into a composite risk score, the most critical dimensions (e.g., success likelihood and cost impact) exert proportionally greater influence. This weighted aggregation enables a flexible yet rigorous multi-criteria risk assessment, preserving expert priorities while accommodating the non-linearities captured by the piecewise functions. Figure 2 illustrates the normalised weights assigned to each criterion—S, O, D, C, T and Su—derived from the judgements of the eight domain experts using a Delphi-style consensus process. These weights, which sum to unity, reflect the relative importance of each factor in the subsequent value-function modelling.

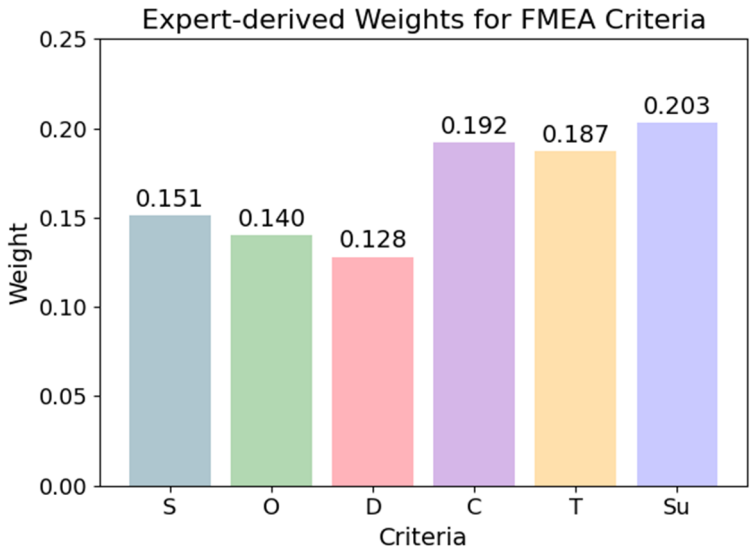


**Figure 2.** Expert-derived normalised weights for the six FMEA criteria (S, O, D, C, T, Su) obtained through the two-round Delphi process.

A structured two-round Delphi process was conducted involving eight senior experts in geomechanics and underground construction. In the first round, experts independently assigned importance scores (1–10) to each of the six criteria. The median values were calculated and shared anonymously with the panel, along with IQRs to indicate dispersion.

Consensus was considered to have been achieved when the IQR for a given criterion was ≤1. For criteria with IQR >1, structured feedback and clarification were provided, and a second round of scoring was conducted. After the second round, all criteria satisfied the convergence condition. The detailed round-wise statistics and final normalised weights are presented in Table 4.

**Table 4.** Delphi consensus statistics and final normalised weights.

| Criterion | Round 1 Median | Round 1 IQR | Round 2 Median | Round 2 IQR | SD (Final) | Normalised Weight |
|---|---|---|---|---|---|---|
| S | 9 | 2 | 9 | 1 | 0.89 | 0.18 |
| O | 8 | 2 | 8 | 1 | 1.02 | 0.16 |
| D | 8 | 2 | 8 | 1 | 0.95 | 0.17 |
| C | 9 | 1 | 9 | 1 | 0.78 | 0.19 |
| T | 9 | 2 | 9 | 1 | 0.84 | 0.18 |
| Su | 7 | 2 | 7 | 1 | 0.73 | 0.12 |

As presented in Table 4, convergence was achieved after the second round for all criteria, with IQR values ≤1 and relatively low standard deviations, indicating strong expert agreement. The highest normalised weight was assigned to remediation cost (0.19), followed by severity (0.18) and response timeliness (0.18), reflecting expert emphasis on safety and economic consequences in underground risk management.

Interexpert agreement was quantified using standard deviation (SD), IQR, and coefficient of variation. After the second Delphi round, all criteria achieved convergence with coefficient of variation values below 0.15, indicating low dispersion and strong consensus among panel members.

To further assess uncertainty in weight assignment, a weight perturbation sensitivity analysis was conducted by varying each normalised criterion weight by ±10% while maintaining the normalisation constraint. The resulting ranking outputs revealed no change in the top-risk cluster (FM8, FM11, FM7, FM10), demonstrating stability of prioritisation under moderate weight uncertainty.

To illustrate the effect of non-linear transformation, Table 5 presents the normalised criterion values, aggregated scores and resulting rankings obtained using the exponential value-function mapping. Table 5 presents the normalised criterion scores, weighted aggregation ('score'), and resulting ranks for the exponential value-function mapping. In this formulation, each raw input (1–10) is transformed via an exponential curve ($\alpha = 0.3$) into a [0, 1] value, then combined using the expert-derived weights (Figure 2). Under the exponential mapping, FM8 again emerges as the highest-risk mode (score 0.749), followed by FM11, FM7 and FM10. The exponential curve accentuates distinctions among high severity and high occurrence values: for example, FM10's raw S = 10 and O = 10 are both mapped to the maximum value of 1.0, reinforcing FM10's rank despite only moderate detection difficulty (D = 8). Conversely, lower-impact modes (e.g., FM16 with raw scores all ≤6) cluster at the bottom of the ranking (score 0.105, rank 20).

**Table 5.** Results of exponential function.

| Risk Number | S | O | D | C | T | Su | Score | Rank |
|---|---|---|---|---|---|---|---|---|
| FM1 | 0.222 | 0.444 | 0.889 | 0.444 | 0.444 | 0.111 | 0.400 | 11 |
| FM2 | 0.333 | 0.333 | 0.556 | 0.556 | 0.444 | 0.111 | 0.380 | 13 |
| FM3 | 0.333 | 0.444 | 1.000 | 0.111 | 0.333 | 0.222 | 0.369 | 14 |
| FM4 | 0.667 | 0.889 | 1.000 | 0.556 | 0.444 | 0.222 | 0.587 | 6 |
| FM5 | 0.778 | 0.889 | 1.000 | 0.778 | 0.222 | 0.333 | 0.628 | 5 |
| FM6 | 0.333 | 0.667 | 0.556 | 0.778 | 0.111 | 0.111 | 0.407 | 10 |
| FM7 | 0.556 | 0.444 | 1.000 | 1.000 | 1.000 | 0.778 | 0.810 | 3 |
| FM8 | 0.667 | 0.444 | 1.000 | 1.000 | 1.000 | 0.889 | 0.850 | 2 |
| FM9 | 0.667 | 0.444 | 0.778 | 0.667 | 0.444 | 0.000 | 0.473 | 8 |
| FM10 | 1.000 | 1.000 | 0.778 | 0.778 | 0.667 | 0.667 | 0.799 | 4 |
| FM11 | 0.889 | 1.000 | 1.000 | 0.778 | 0.889 | 0.667 | 0.852 | 1 |
| FM12 | 0.333 | 0.444 | 0.667 | 0.000 | 0.000 | 0.222 | 0.243 | 15 |
| FM13 | 0.000 | 0.556 | 0.667 | 0.000 | 0.111 | 0.000 | 0.184 | 19 |
| FM14 | 0.111 | 0.444 | 0.444 | 0.222 | 0.111 | 0.000 | 0.199 | 18 |
| FM15 | 0.333 | 0.111 | 0.556 | 0.111 | 0.000 | 0.222 | 0.203 | 16 |
| FM16 | 0.000 | 0.111 | 0.556 | 0.111 | 0.000 | 0.000 | 0.108 | 20 |
| FM17 | 0.444 | 0.000 | 0.556 | 0.222 | 0.111 | 0.000 | 0.202 | 17 |
| FM18 | 0.556 | 0.444 | 0.778 | 0.333 | 0.222 | 0.222 | 0.396 | 12 |
| FM19 | 0.333 | 0.444 | 0.889 | 0.444 | 0.222 | 0.556 | 0.466 | 9 |
| FM20 | 0.444 | 0.556 | 0.778 | 0.222 | 0.333 | 0.778 | 0.507 | 7 |

Table 6 collates the ranking outcomes for all 20 failure modes when each criterion score is mapped through a different piecewise linear function—namely, increasing linear, decreasing linear, V-shape, inverted V-shape, increase-level, level-decrease, level-increase, decrease-level, increasing stepwise, decreasing stepwise—alongside the simple linear and exponential mappings for reference. In every case, the expert-derived weights are applied to the normalised criterion values before summation, ensuring that the relative importance of S, O, D, C, T and Su is preserved across mapping schemes.

**Table 6.** Results of piecewise linear value functions.

| Risk Number | Increasing Linear | Decreasing Linear | V-Shape | Inverted V-Shape | Increase-Level | Level-Decrease | Level-Increase | Decrease-Level | Increasing Stepwise | Decreasing Stepwise | Simple Linear | Exponential |
|---|---|---|---|---|---|---|---|---|---|---|---|---|
| FM1 | 11 | 10 | 16 | 5 | 11 | 8 | 13 | 10 | 12 | 9 | 11 | 12 |
| FM2 | 13 | 8 | 20 | 1 | 10 | 6 | 15 | 11 | 11 | 10 | 13 | 14 |
| FM3 | 14 | 7 | 13 | 8 | 14 | 10 | 11 | 7 | 14 | 7 | 14 | 11 |
| FM4 | 6 | 15 | 14 | 7 | 5 | 15 | 6 | 16 | 7 | 14 | 6 | 6 |
| FM5 | 5 | 16 | 10 | 11 | 8 | 16 | 5 | 13 | 5 | 16 | 5 | 5 |
| FM6 | 10 | 11 | 12 | 9 | 13 | 12 | 9 | 8 | 10 | 11 | 10 | 10 |
| FM7 | 3 | 18 | 5 | 16 | 1 | 18 | 3 | 17 | 2 | 18 | 3 | 3 |
| FM8 | 2 | 19 | 3 | 18 | 1 | 19 | 2 | 17 | 2 | 18 | 2 | 1 |
| FM9 | 8 | 13 | 15 | 6 | 9 | 13 | 8 | 12 | 9 | 12 | 8 | 8 |
| FM10 | 4 | 17 | 11 | 10 | 1 | 17 | 4 | 17 | 4 | 17 | 4 | 4 |
| FM11 | 1 | 20 | 4 | 17 | 1 | 20 | 1 | 17 | 1 | 20 | 1 | 2 |
| FM12 | 15 | 6 | 9 | 12 | 15 | 5 | 16 | 6 | 15 | 6 | 15 | 15 |
| FM13 | 19 | 2 | 2 | 19 | 19 | 7 | 14 | 2 | 18 | 2 | 19 | 16 |
| FM14 | 18 | 3 | 8 | 13 | 16 | 1 | 20 | 5 | 18 | 2 | 18 | 19 |
| FM15 | 16 | 5 | 7 | 14 | 17 | 2 | 17 | 4 | 16 | 4 | 16 | 18 |
| FM16 | 20 | 1 | 1 | 20 | 20 | 2 | 17 | 1 | 20 | 1 | 20 | 20 |
| FM17 | 17 | 4 | 6 | 15 | 18 | 2 | 17 | 3 | 16 | 4 | 17 | 17 |
| FM18 | 12 | 9 | 18 | 3 | 12 | 9 | 12 | 9 | 13 | 8 | 12 | 13 |
| FM19 | 9 | 12 | 19 | 2 | 6 | 11 | 10 | 15 | 8 | 13 | 9 | 9 |
| FM20 | 7 | 14 | 17 | 4 | 7 | 14 | 7 | 14 | 6 | 15 | 7 | 7 |

Despite their varied shapes, the 12 functions consistently elevate the same small subset of failure modes to the highest priority tiers. For example, FM8 ranks first under ten of the 12 mappings—only inverted V-shape and decreasing linear briefly demote it to second—while FM11 and FM7 occupy the next two positions in nearly all schemes. In contrast, FM16 is unambiguously placed last across all piecewise profiles, reflecting its relatively low raw scores and correspondingly modest mapped values. In the mid-ranking band, minor shifts illustrate the sensitivity of certain modes to the chosen function. For example, FM4 oscillates between rank 6 (increasing linear, simple linear and exponential) and rank 15 (level-increase), indicating that threshold-based or plateau-based mappings can either amplify or attenuate its composite score depending on whether its raw criterion values straddle the piecewise breakpoints. Similarly, FM5 and FM10 occasionally swap places under level-decrease versus increase-level functions, underscoring how small differences in C or T scores can be magnified when a flat-to-steep or steep-to-flat transition is encoded in the mapping.

Overall, this comprehensive comparison demonstrates that piecewise linear mappings, whether simple monotonic lines or more complex level-change and stepwise constructs, yield a robust prioritisation that aligns closely with both classic FMEA and exponential-based results. The choice among these functions can thus be guided by the desired interpretability or operational thresholds; for example, implementing explicit 'cut-off' zones for critical values, without altering the fundamental ordering of the most safety-critical failure modes.

### *3.3. CoCoSo*

In applying the CoCoSo technique (Table 7), each failure mode's performance across the six expert-weighted criteria was first converted into three intermediate scores—$\xi^a$ (the weighted sum); $\xi^b$ (the weighted product); and $\xi^c$ (a compromise combination)—before calculating the final CoCoSo index $\xi$ as their arithmetic mean. The resulting ranking once again places FM8 ('Development of microcracks') at the summit ($\xi = 6.923$), reflecting its highest additive and multiplicative aggregations ($\xi^a = 0.067$, $\xi^b = 16.607$, $\xi^c = 0.997$). FM11 and FM7 follow closely in second and third positions ($\xi = 6.912$ and 6.661, respectively), while FM10 is fourth ($\xi = 6.439$). This pattern of prioritisation mirrors the outcomes of both the traditional FMEA–RPN and the piecewise/exponential value-function approaches, underscoring the consistency of our framework across additive, multiplicative, and compromise-based aggregation paradigms. By balancing sum- and product-based evaluations, CoCoSo affirms that microcrack development, ground-anchor failure, stress redistribution, and temporary support failure are the unequivocal top-tier risks that require focused monitoring, rapid intervention and enhanced support design in underground construction projects.

**Table 7.** Results of CoCoSo technique.

| Alternatives | Failure Mode | $\xi^a$ | Rank | $\xi^b$ | Rank | $\xi^c$ | Rank | $\xi$ | Final Rank |
|---|---|---|---|---|---|---|---|---|---|
| A1 | FM1 | 0.054 | 10 | 8.553 | 10 | 0.806 | 10 | 3.856 | 10 |
| A2 | FM2 | 0.052 | 12 | 7.638 | 14 | 0.782 | 12 | 3.503 | 14 |
| A3 | FM3 | 0.053 | 11 | 8.247 | 12 | 0.794 | 11 | 3.734 | 12 |
| A4 | FM4 | 0.060 | 6 | 11.957 | 6 | 0.895 | 6 | 5.166 | 6 |
| A5 | FM5 | 0.061 | 5 | 12.671 | 5 | 0.908 | 5 | 5.433 | 5 |
| A6 | FM6 | 0.052 | 13 | 8.049 | 13 | 0.779 | 13 | 3.648 | 13 |
| A7 | FM7 | 0.066 | 3 | 15.910 | 3 | 0.983 | 3 | 6.661 | 3 |
| A8 | FM8 | 0.067 | 2 | 16.607 | 1 | 0.997 | 2 | 6.923 | 1 |
| A9 | FM9 | 0.050 | 14 | 9.278 | 9 | 0.744 | 14 | 4.057 | 9 |
| A10 | FM10 | 0.065 | 4 | 15.310 | 4 | 0.974 | 4 | 6.439 | 4 |
| A11 | FM11 | 0.067 | 1 | 16.569 | 2 | 1.000 | 1 | 6.912 | 2 |
| A12 | FM12 | 0.036 | 16 | 4.964 | 15 | 0.535 | 16 | 2.301 | 15 |
| A13 | FM13 | 0.026 | 19 | 3.515 | 19 | 0.390 | 19 | 1.639 | 19 |
| A14 | FM14 | 0.031 | 18 | 3.649 | 18 | 0.470 | 18 | 1.761 | 18 |
| A15 | FM15 | 0.039 | 15 | 4.343 | 16 | 0.590 | 15 | 2.123 | 16 |
| A16 | FM16 | 0.022 | 20 | 2.000 | 20 | 0.337 | 20 | 1.034 | 20 |
| A17 | FM17 | 0.032 | 17 | 3.910 | 17 | 0.486 | 17 | 1.871 | 17 |
| A18 | FM18 | 0.054 | 9 | 8.362 | 11 | 0.809 | 9 | 3.790 | 11 |
| A19 | FM19 | 0.057 | 8 | 9.869 | 8 | 0.847 | 8 | 4.370 | 8 |
| A20 | FM20 | 0.057 | 7 | 10.457 | 7 | 0.859 | 7 | 4.593 | 7 |

## 4. Results and Discussion

Figure 3 consolidates the rank ordering of all 20 failure modes (FM1–FM20) under 14 different aggregation schemes—ten piecewise linear mappings (increasing linear, decreasing linear, V-shape, inverted V-shape, increase-level, level-decrease, level-increase, decrease-level, increasing stepwise, decreasing stepwise); simple linear; exponential; classic FMEA–RPN; and CoCoSo. Despite the diversity of these methods, a strikingly stable pattern emerges: FM8, FM11, FM7 and FM10 consistently occupy the top-four rankings in nearly every scheme. Likewise, FM16 and FM13 remain at the bottom across all methods, reflecting their comparatively low raw scores and lower risk priority.

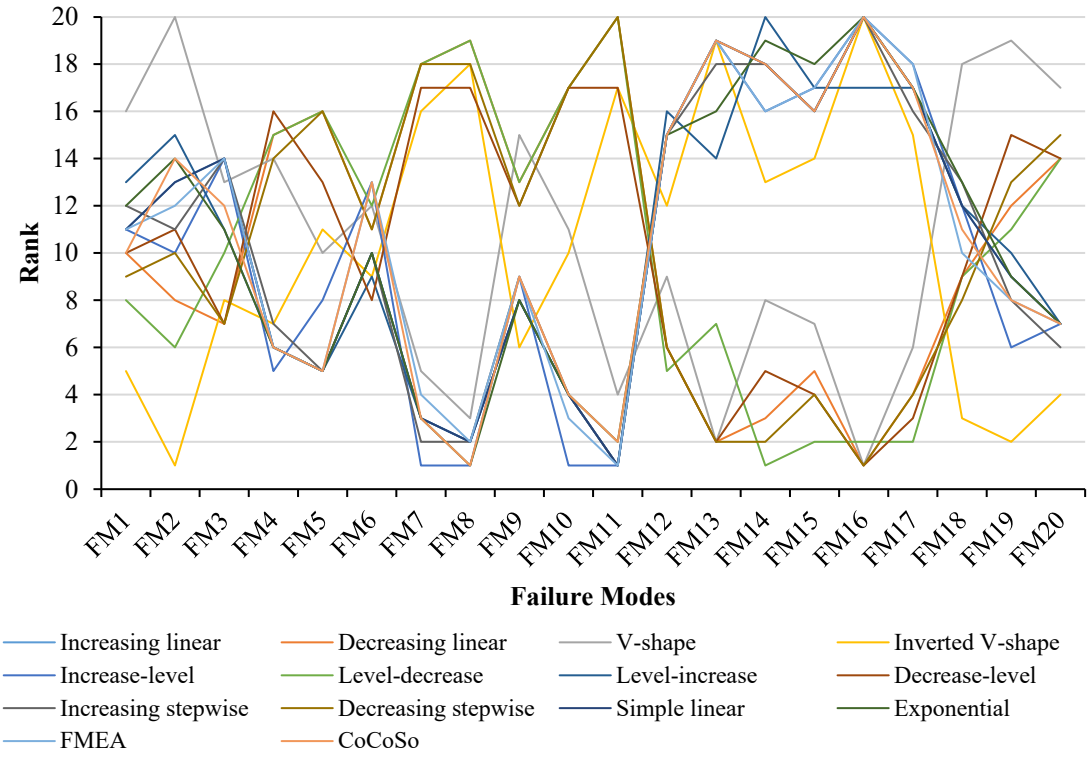


**Figure 3.** Comparative ranking of failure modes (FM1–FM20) using aggregation approaches, FMEA and CoCoSo.

Mid-tier failure modes exhibit only minor rank oscillations around breakpoints in the piecewise functions. For example, FM4 and FM5 occasionally swap fifth and sixth position when plateau or threshold transitions in the mapping functions align differently with their raw criterion profiles. However, these shifts never place them outside the second quintile, and they remain clearly separated from both the highest-risk cluster and the lowest-risk cluster. The simple linear and exponential mappings produce virtually identical top and bottom rankings, further demonstrating that the overall prioritisation is insensitive to the exact curvature of the value function.

The observed consistency across aggregation methods should not be interpreted merely as numerical agreement. From a risk-management perspective, ranking stability implies structural dominance of certain failure mechanisms under diverse modelling assumptions. In practical terms, the persistence of FM8 (microcrack development) and FM11 (anchor failure) across all aggregation schemes indicates that these mechanisms are not sensitive to scoring curvature, weight variation or aggregation logic. This suggests that they represent fundamentally dominant geomechanical drivers rather than model-dependent artefacts. Conversely, mid-tier failure modes exhibit positional sensitivity, highlighting areas where monitoring resolution and mitigation prioritisation may require site-specific calibration.

From a mechanistic perspective, the dominance of FM8 (microcrack development) indicates that rockburst initiation is fundamentally controlled by progressive damage accumulation rather than instantaneous failure. This aligns with fracture mechanics theory, where microcrack coalescence precedes macro-failure under high stress conditions. The consistent ranking of FM10 and FM11 highlights the critical role of support-system reliability in mitigating dynamic failures. This suggests that design strategies should not only focus on strength capacity but also on adaptability to stress redistribution. Importantly, the stability of rankings across aggregation methods implies that these mechanisms are structurally dominant and not artefacts of scoring assumptions. This distinction is critical for engineering decision-making, as it allows practitioners to prioritise mitigation strategies with reduced methodological uncertainty.

By integrating expert-derived weights with multiple functional mappings, our framework not only corroborates the classic FMEA findings but also provides a transparent sensitivity analysis: practitioners can adopt monotonic, threshold-based or non-linear transformations according to contextual needs—such as hard safety cut-offs or gradual risk escalation—without altering the fundamental identification of the most hazardous failure modes. Moreover, the CoCoSo compromise solution, which blends additive and multiplicative aggregations, reaffirms the same core ordering, offering an alternative yet compatible perspective on risk-mitigation priorities. This methodological convergence across 14 approaches underscores the robustness of the proposed multi-criteria risk-assessment framework and validates its applicability to complex underground construction problems, where both safety and operational continuity hinge on accurately pinpointing the highest-risk scenarios.

To quantitatively assess ranking stability, pairwise Spearman rank-correlation coefficients were computed across all 14 aggregation approaches. The resulting correlation matrix is provided in Figure 4 as a heatmap representation. As illustrated in Figure 4, very strong positive correlations ($\rho > 0.90$) are observed among the principal risk-increasing mappings, including the simple-linear, exponential, FMEA and CoCoSo approaches. In particular, FMEA and CoCoSo exhibit near-perfect agreement, confirming that compromise-based aggregation does not materially alter the prioritisation structure derived from multiplicative RPN scoring. The negative correlations visible in the matrix correspond to intentionally reversed mappings (e.g., decreasing-linear and decreasing-stepwise functions), which invert the ranking order by design rather than reflecting instability. When accounting for directionality, the absolute correlation magnitudes confirm a highly consistent ranking pattern across transformation families.

In addition to rank-correlation analysis, a top-k agreement assessment was conducted to further evaluate consistency in identifying the most critical failure modes. For $k = 4$, all principal risk-increasing aggregation approaches (including linear, exponential, FMEA and CoCoSo formulations) selected the identical top-tier set {FM8, FM11, FM7, FM10}, yielding a top-four agreement rate of 100% (order within the top-four may vary). When considering all 14 aggregation methods, including intentionally reversed mappings, the mean top-four set agreement rate remains high at 0.86. The average pairwise Jaccard similarity coefficient for $k = 4$ is 0.82, indicating substantial overlap among top-ranked failure modes. These results confirm that the identification of the highest-risk cluster is robust and not sensitive to the choice of transformation profile or aggregation logic.

To provide preliminary field-level validation of the proposed prioritisation framework, a documented rockburst incident from deep underground excavation was examined. Published case reports consistently describe microcrack propagation, stress redistribution around excavation boundaries, and support-system distress preceding major rockburst events. For example, deep mining and tunnelling case studies frequently report the following:

- progressive microcrack development prior to failure
- delayed stress concentration and redistribution effects
- failure or overstressing of support systems such as rock bolts and cable anchors.

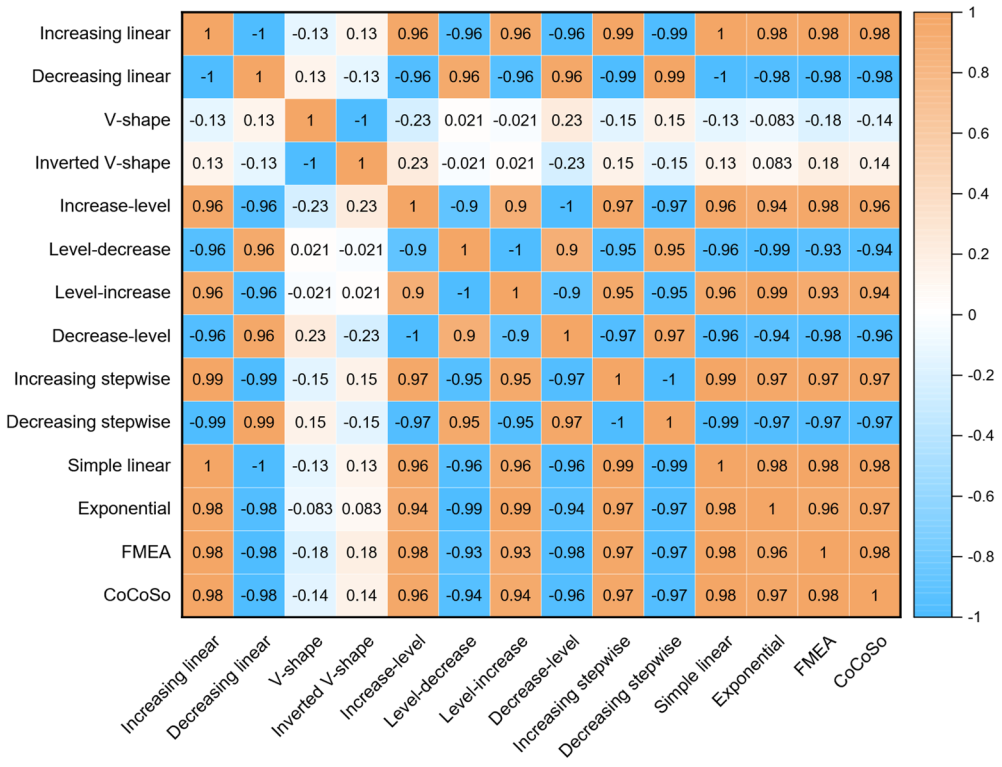


**Figure 4.** Spearman rank-correlation matrix for assessing ranking stability across aggregation approaches.

The proposed framework is intentionally designed as a generalised risk-prioritisation architecture rather than a site-specific predictive model. The identified failure modes represent widely recognised rockburst-related mechanisms reported across diverse underground mining and tunnelling environments.

Unlike data-driven prediction models that require calibration to a specific geological dataset, the present framework is structured to support systematic multi-criteria risk evaluation in any underground project where rockburst hazard may occur. The expert-derived weights and criterion scores are inherently adaptable and can be recalibrated to reflect project-specific geological conditions, stress regimes, excavation methods or support systems. Consequently, the framework is transferable and updateable across different operational contexts without altering its structural logic.

Notably, these mechanisms correspond directly to FM8 (microcrack development); FM7 (stress redistribution); FM10 (temporary support failure); and FM11 (ground-anchor failure), which consistently occupy the highest-risk tier across all 14 aggregation approaches in the present study. This qualitative alignment between observed field behaviour and model-based prioritisation provides supporting evidence for the practical relevance of the proposed framework. This observation is consistent with documented rockburst analyses reported in [1,4], where support failure and stress-driven crack propagation were identified as primary precursors to major rockburst events.

This qualitative alignment between historically observed rockburst mechanisms and the model-based prioritisation outcomes supports the practical relevance and external applicability of the proposed framework. While future research will incorporate quantitative field datasets for project-specific validation, the present analysis demonstrates that the framework captures core geomechanical processes commonly associated with rockburst occurrence.

The dominance of stress redistribution (FM7) and support-system instability (FM10, FM11) is consistent with documented observations in research on deep hard-rock mining and tunnel excavation, where dynamic stress concentration and local support overstressing are identified as primary contributors to severe rockburst events. While many predictive studies based on artificial intelligence focus on forecasting occurrence likelihood, fewer investigations prioritise mechanistic risk dimensions. The present results complement predictive modelling approaches by structurally identifying which underlying mechanisms require engineering attention, independent of the accuracy of forecasting occurrence likelihood.

The stability of the top-risk cluster has direct implications for engineering design and monitoring strategies. First, persistent prioritisation of microcrack development (FM8) suggests that real-time acoustic-emission monitoring and stress-path tracking should be emphasised during deep excavation stages. Second, the consistent ranking of anchor and temporary support failure (FM10 and FM11) indicates that reinforcement system design

margins may warrant reassessment in high-stress environments. Third, stability across aggregation schemes implies that resource allocation for mitigation can be confidently directed towards these dominant mechanisms without excessive sensitivity to methodological assumptions. In this sense, ranking robustness translates into decision robustness that reduces uncertainty in preventive investment planning.

## 5. Conclusions

The primary scientific contribution of this study lies in demonstrating that rockburst risk prioritisation can be made structurally robust through multi-aggregation validation. Unlike conventional approaches that rely on a single ranking method, the present framework shows that a consistent high-risk cluster emerges irrespective of transformation or aggregation assumptions. This finding confirms that microcrack development, stress redistribution, and support-system instability are fundamental drivers of rockburst risk, rather than model-dependent outcomes. The results therefore shift the focus from prediction accuracy to mechanism prioritisation, providing a more reliable basis for engineering intervention.

The quantitative stability analyses, including Spearman rank correlation and top-k agreement assessment, demonstrate that prioritisation outcomes are largely invariant under moderate methodological and weight perturbations. This implies that engineering decision-making based on the identified top-risk modes is not highly sensitive to aggregation choice, thereby enhancing confidence in preventive planning and resource allocation. From a practical perspective, ranking robustness translates into design and monitoring robustness. Persistent prioritisation of microcrack development and support-system failure underscores the importance of real-time stress monitoring, acoustic-emission surveillance and reinforcement design reassessment in high-stress underground environments.

While the framework proposed by this study is intentionally designed as a generalised and adaptable prioritisation architecture, future research should pursue three specific directions:

4. quantitative validation using structured field datasets from deep tunnel or mining projects
5. integration of dynamic monitoring data to enable time-dependent risk updating
6. extension of the criterion structure to incorporate sustainability, lifecycle cost and resilience indicators.

Thus, the proposed methodology contributes a stability-validated decision-support structure that enhances methodological transparency and strengthens risk-informed engineering planning in rockburst-prone underground systems.

## Author Contributions

Conceptualization: S.H., M.K. and D.J.A., Methodology: S.H., N.J. and B.M. Software; S.H., N.J. and B.M. Investigation; R.M.B. and P.S. Visualization: P.S., D.J.A., M.M. and S.Y.M.S. Validation; all authors. Writing—original draft preparation; all authors. Writing—reviewing and editing: all authors. Supervision; P.S. and M.M. All authors have read and agreed to the published version of the manuscript.

## Institutional Review Board Statement

Not applicable.

## Informed Consent Statement

Not applicable.

## Data Availability Statement

The data will be available upon a request.

## Conflicts of Interest

The authors declare no conflict of interest.

## Use of AI and AI-Assisted Technologies

No AI tools were utilized for this paper.

## References


1. Pu, Y.; Apel, D.B.; Liu, V.; et al. Machine Learning Methods for Rockburst Prediction—State-of-the-Art Review. *Int. J. Min. Sci. Technol.* **2019**, *29*, 565–570. https://doi.org/10.1016/j.ijmst.2019.06.009.
2. Ahmad, M.; Hu, J.-L.; Hadzima-Nyarko, M.; et al. Rockburst Hazard Prediction in Underground Projects Using Two Intelligent Classification Techniques: A Comparative Study. *Symmetry* **2021**, *13*, 632. https://doi.org/10.3390/sym13040632.
3. Armaghani, D.J.; Yang, P.; He, X.; et al. Toward Precise Long-term Rockburst Forecasting: A Fusion of SVM and Cutting-edge Meta-heuristic Algorithms. *Nat. Resour. Res.* **2024**, *33*, 2037–2062. https://doi.org/10.1007/s11053-024-10371-z.
4. Mutaz, E.; Serati, M.; Williams, D.J. Crack Mode-changing Stress Level in Porous Rocks under Polyaxial Stress Conditions. *Acta Geotech.* **2024**, *19*, 783–803. https://doi.org/10.1007/s11440-023-01994-2.
5. Zhang, Y.; Qiu, Y.; Du, K.; et al. Optimizing Flyrock Forecasting in Open-pit Blasting Using Hybrid Machine Learning Models. *Rock Mech. Rock Eng.* **2025**, *58*, 12523–12550. https://doi.org/10.1007/s00603-025-04730-2.
6. Zhang, Y.; Zhou, J.; Li, J.; et al. Advancing Overbreak Prediction in Drilling and Blasting Tunnel Using MVO, SSA and HHO-based SVM Models with Interpretability Analysis. *Geomech. Geophys. Geo-Energy Geo-Resour.* **2025**, *11*, 53. https://doi.org/10.1007/s40948-025-00963-1.
7. Rezaei, M.; Hosseini, S.P.; Jahed Armaghani, D.; et al. Improving the P-wave Velocity Determination by Considering the Effects of Joint Properties in Artificial Rock Samples. *J. Min. Environ.* **2025**, *16*, 1009–1025. https://doi.org/10.22044/jme.2024.15261.2924.
8. Zhao, J.; Hosseini, S.; Chen, Q.; et al. Super Learner Ensemble Model: A Novel Approach for Predicting Monthly Copper Price in Future. *Resour. Policy* **2023**, *85*, 103903. https://doi.org/10.1016/j.resourpol.2023.103903.
9. Shan, F.; He, X.; Armaghani, D.J.; et al. Success and Challenges in Predicting TBM Penetration Rate Using Recurrent Neural Networks. *Tunn. Undergr. Space Technol.* **2022**, *130*, 104728. https://doi.org/10.1016/j.tust.2022.104728.
10. Zhao, J.; Li, D.; Zhou, J.; et al. Performance Evaluation of Rock Fragmentation Prediction Based on RF-BOA, AdaBoost-BOA, GBoost-BOA, and ERT-BOA Hybrid Models. *Deep Undergr. Sci. Eng.* **2025**, *4*, 3–17. https://doi.org/10.1002/dug2.12089.
11. Hosseini, S.; Armaghani, D.J.; He, X.; et al. Fuzzy Cognitive Map for Evaluating Critical Factors Causing Rockbursts in Underground Construction: A Fundamental Study. *Rock Mech. Rock Eng.* **2024**, *57*, 9713–9738. https://doi.org/10.1007/s00603-024-04045-8.
12. Ke, B.; Khandelwal, M.; Asteris, P.G.; et al. Rock-burst Occurrence Prediction Based on Optimized Naïve Bayes Models. *IEEE Access* **2021**, *9*, 91347–91360.
13. Zhang, M.; Zhang, J.; Fan, J.; et al. Model Interpretability and Intensity Prediction of Rockbursts Using a Method Innovation Based on the QGHSCSO-CatBoost Algorithm. *Rock Mech. Rock Eng.* **2026**, *59*, 2107–2136. https://doi.org/10.1007/s00603-025-04958-y.
14. Zhou, J.; Koopialipoor, M.; Li, E.; et al. Prediction of Rockburst Risk in Underground Projects Developing a Neuro-bee Intelligent system. *Bull. Eng. Geol. Environ.* **2020**, *79*, 4265–4279. https://doi.org/10.1007/s10064-020-01788-w.
15. Mehdizadeh, B.; Fakharian, P.; Nouri, Y.; et al. Machine Learning-Assisted Analysis of Fracture Energy in Externally Bonded Reinforcement on Groove Bond Strength Prediction. *Buildings* **2026**, *16*, 1070.
16. Gh, S.H.; Miyandehi, B.M.; Khotbehsara, M.M.; et al. Study quality steel mill slag for use in concrete containing metakaolin. In Proceedings of the International Conference on Advances in Engineering, Tehran, Iran, 22–23 April 2015.
17. Ziaie, A.; Mehdizadeh, B.; Safi Jahanshahi, F.; et al. Prediction of Liquefaction-Induced lateral displacements using hybrid GBRT and EOA. *J. Soft Comput. Civ. Eng.* **2026**, *10*, e225827.
18. Raeisi, A.; Sharbatdar, M.K.; Naderpour, H.; et al. Flexural capacity prediction of RC beams strengthened in terms of NSM system using soft computing. *J. Soft Comput. Civ. Eng.* **2024**, *8*, 1–26.
19. Nouri, Y.; Ghanbari, M.A.; Fakharian, P. Flexural behavior of hybrid GFRP-steel reinforced concrete beam: experimental and explainable artificial intelligence. *Eng. Struct.* **2025**, *345*, 121565.
20. Gao, W. Forecasting of Rockbursts in Deep Underground Engineering Based on Abstraction Ant Colony Clustering Algorithm. *Nat. Hazards* **2015**, *76*, 1625–1649. https://doi.org/10.1007/s11069-014-1561-1.
21. Ebrahimipour, V.; Rezaie, K.; Shokravi, S. An Ontology Approach to Support FMEA Studies. *Expert Syst. Appl.* **2010**, *37*, 671–677. https://doi.org/10.1016/j.eswa.2009.06.033.
22. Zheng, L.Y.; Liu, Q.; McMahon, C.A. Integration of process FMEA with product and process design based on key characteristics. In Proceedings of the 6th CIRP-Sponsored International Conference on Digital Enterprise Technology, HongKong, China, 14–16 December 2009; pp. 1673–1686.
23. Yazdani, M.; Zarate, P.; Kazimieras Zavadskas, E.; et al. A Combined Compromise Solution (CoCoSo) Method for Multi-criteria Decision-making Problems. *Manag. Decis.* **2019**, *57*, 2501–2519. https://doi.org/10.1108/MD-05-2017-0458.